JACS
JOURNAL OF THE AMERICAN CHEMICAL SOCIETY

Article

Aqueous Solvation of Ammonia and Ammonium: Probing Hydrogen Bond Motifs with FT-IR and Soft-X-Ray Spectroscopy

Maria Ekimova, Wilson Quevedo, Lukasz Szyc, Marcella Iannuzzi, Philippe Wernet, Michael Odelius, and Erik T. J. Nibbering

J. Am. Chem. Soc., **Just Accepted Manuscript** • DOI: 10.1021/jacs.7b07207 • Publication Date (Web): 15 Aug 2017

ACS Publications

Journal of the American Chemical Society is published by the American Chemical Society. 1155 Sixteenth Street N.W., Washington, DC 20036

Aqueous Solvation of Ammonia and Ammonium: Probing Hydrogen Bond Motifs with FT-IR and Soft-X-Ray Spectroscopy

Maria Ekimova[1], Wilson Quevedo[2], Łukasz Szyc[3], Marcella Iannuzzi[4], Philippe Wernet[2], Michael Odelius[5], Erik T. J. Nibbering[1]

[1]Max Born Institute for Nonlinear Optics and Short Pulse Spectroscopy, Max Born Str. 2A, 12489 Berlin, Germany.
[2] Institute for Methods and Instrumentation for Synchrotron Radiation Research, Helmholtz-Zentrum Berlin für Materialien und Energie GmbH, Albert-Einstein-Strasse 15, 12489 Berlin, Germany.
[3]Magnosco c/o LTB Lasertechnik Berlin GmbH, Am Studio 2c, 12489 Berlin, Germany.
[4] Institute of Physical Chemistry, University of Zurich, Winterthurerstrasse 190, CH-8057 Zurich, Switzerland.
[5] Department of Physics, Stockholm University, AlbaNova University Center, 106 91 Stockholm, Sweden.

Email: nibberin@mbi-berlin.de ; odelius@fysik.su.se ; wernet@helmholtz-berlin.de

Abstract

In a multi-facetted investigation combining local soft-x-ray and vibrational spectroscopic probes with ab initio molecular dynamics simulations, hydrogen-bond interactions of two key principal amine compounds in aqueous solution, ammonia (NH_3) and ammonium ion (NH_4^+), are quantitatively assessed in terms of electronic structure, solvation structure, and dynamics. From the x-ray measurements and from the complementary determination of the IR-active hydrogen stretching and bending modes of NH_3 and NH_4^+ in aqueous solution, the picture emerges of a comparatively strongly hydrogen-bonded NH_4^+ ion via N-H donating interactions, whereas NH_3 has a strong accepting hydrogen bond with one water molecule at the nitrogen lone pair but only weak N-H donating hydrogen bonds. In contrast to the case of hydrogen bonding amongst solvent water molecules, we find that energy mismatch between occupied orbitals of both the solutes NH_3 and NH_4^+ and the surrounding water prevents strong mixing between orbitals upon hydrogen bonding, and –thus – inhibits substantial charge transfer between solute and solvent. A close inspection of the calculated unoccupied molecular orbitals, in conjunction with experimentally measured N K-edge absorption spectra, reveals the different nature of the electronic structural effects of these two key principal amine compounds imposed by hydrogen bonding to water, where a p*H*-dependent excitation energy appears to be an intrinsic property. These results provide a benchmark for hydrogen bonding of other nitrogen containing acids and bases.

1. Introduction

Ammonia (NH_3) and ammonium ion (NH_4^+), crucial constituents in the nitrogen cycle,[1] are the smallest nitrogen containing compounds with the capacity of forming hydrogen bonds. Being ideal testing systems for understanding hydrogen bond interactions, the role of hydrogen bonding for NH_3 and NH_4^+ in aqueous solutions has been topic of intense scientific debate. Simulations of NH_4^+(aq) has received a large attention due to the strong interactions and influence of quantum effects.[2-7] Whereas NH_4^+ is now understood to donate hydrogen bonds to four water molecules within the first solvent shell, another fifth water molecule is also closely associated with the hydrated NH_4^+ ion,[2-11] affecting the rotational dynamics of aqueous NH_4^+. Results from other QM/MM simulations have, however, suggested a weaker interaction and free rotation of the NH_4^+ ion.[10] Evaluation of different computation approximations indicate that Density Functional Theory (DFT) simulations tend to overestimate the interaction strength between the NH_4^+ ion and water further complicating the picture.[5] In contrast, the situation for aqueous NH_3 is much less clear: NH_3 is understood to accept hydrogen bonds with water through its lone pair forming a molecular complex H−O−H···NH_3 with a comparatively strong hydrogen bond, as gas phase cluster measurements indeed confirm,[12-14] albeit that QM/MM calculations suggest a coordination number larger than one for the NH_3 lone pair.[11,15] Liquid NH_3 may also serve as a reference for hydrogen bonding of NH_3 and coordination numbers derived from x-ray and neutron diffraction studies [16-20] point at NH_3 having fewer or weaker donating hydrogen bonds than water. This is in agreement with the results of gas-phase structural studies of NH_3 clusters,[21-23] molecular dynamics (MD) simulations,[24] ab initio Monte Carlo simulations,[25,26] as well as ab initio molecular dynamics calculations.[15,27,28] This notion of weaker hydrogen bonds of NH_3 compared to water challenges the generally accepted textbook knowledge of hydrogen bonding of NH_3 [29-32] as it would entail pure liquid NH_3 to be dominated by steric packing rather than hydrogen bonding.[27] The capacity of NH_3 to donate hydrogen bonds through its N-H groups to the solvent water is not clearly established. Weak hydrogen bonds can be expected to result in an average coordination number less than three with associated hydrogen bond breaking and reformation dynamics on ultrafast time scales rendering the assessment of hydrogen bonding of solvated NH_3 difficult.

Despite the insight into structural details of the hydration of NH_3 and of NH_4^+ in solution provided by x-ray or neutron diffraction,[16-20] NMR spectroscopy,[33,34] QM/MD studies.[2-11,15] gas-phase clusters spectroscopic studies,[12-14,23,35-40] and low-temperature solid matrix or crystalline studies,[41-50] ambiguities on the number and strengths of hydrogen bonds to the solvent water, and the associated hydrogen bond dynamics, remain. This propels the necessity for further experimental evidence on the fundamental nature of hydrogen bonding of NH_3 and of NH_4^+ in solution.

In this work we study the hydrogen bond characteristics of aqueous NH_3 and NH_4^+ by use of two different local probes: Fourier-transform infrared (FT-IR) spectroscopy enables to monitor hydrogen stretching and bending modes,[51] being a renowned method to characterize hydrogen bond interactions and dynamics. [52-61] Soft-x-ray spectroscopy has more recently become a viable tool to probe hydrogen bond interactions, in particular for water,[62-65] but also in the hydration shells of ammonia and amine species.[26,66] We present in this paper results obtained on aqueous NH_3 and NH_4^+ in a combined experimental and theoretical steady-state IR and x-ray spectroscopic approach. MD simulations, spectrum calculations and electronic-structure theory performed using a dispersion corrected BLYP functional in the CP2K software [67] link the experimental insights to geometric structures and bonding – and provide a common ground – also for other experimental probes, for understanding how local interactions are expressed in structure and dynamics of the solutions.

The outline of the paper is as follows. In Section 2 we explore the solvation structure of aqueous NH_3 and NH_4^+ with ab initio molecular dynamics (AIMD) simulations, in terms of radial distribution functions, number of hydrogen bonds, and time scales for hydrogen bond dynamics. We then investigate hydrogen bonding of aqueous NH_3 and NH_4^+ by identifying and characterising the local IR and soft-x-ray marker transitions in Sections 3 and 4, respectively. We use the method of two-dimensional correlation spectroscopy (2D-COS) to overcome the major spectral overlap with the solvent water in the FT-IR spectra, and can unequivocally locate the hydrogen stretching modes of both aqueous NH_3 and NH_4^+ without assumptions imposed on the spectral data analysis. We compare the N K-edge spectra of aqueous NH_3 with existing gas-phase data,[26,66], ammonia ice,[68] ammonia adsorbed on ZnO surfaces,[69] as well as the reported soft x-ray absorption spectrum of aqueous NH_3 derived from RIXS measurements.[26] To interpret our experimental and theoretical results on NH_3(aq) and NH_4^+(aq) in a systematic way, we follow earlier discussions of the K-edge absorption spectra of isoelectronic HF, H_2O, NH_3 and CH_4 in the seminal textbook by Stöhr on NEXAFS spectroscopy (in particular Fig. 4.6 in Ref. [70]) and in the review on XAS of water and ice by Nilsson *et al*..[63] With this approach we show how the hydrogen bonding interactions with the solvent water influence the 1s core excitations giving rise to specific features in the pre-edge, main-edge and post-edge regions, respectively. After exploring the solvation structure, and characterising the vibrational and soft-x-ray spectroscopic transitions, we complete our hydration study of aqueous NH_3 and NH_4^+ in Section 5 with an assessment of the role of hydration in shaping the electronic structure of these two elementary nitrogen compounds, and compare the magnitude of possible charge transfer contributions to the solvent water with previous reports on hydrogen bond interactions in bulk water. With these results we provide new information on two elementary nitrogen containing compounds, benchmarking the hydrogen bonding interactions under aqueous solvation conditions that will be of instructive nature for future studies on hydrated alkylamine and alkylammonium compounds, using these two types of local probing of hydrogen bond structure. In addition

to that our current study provides guidelines how to investigate amine and ammonium functional groups in biomolecular surroundings, e.g. within the context of hydration of or proton transport pathways. Ultimately this work suggests future studies of the dynamics of these hydrogen bonds on ultrafast time scales, using ultrafast IR and soft-x-ray spectroscopy.

2. Solvation Structure of Aqueous NH_4^+ and NH_3

In the top of Figure 1 we show representative snapshots of our MD simulations that illustrate the fundamental differences in hydrogen-bonding configurations and electronic structures of NH_3 and NH_4^+ in aqueous solution from a theoretical and conceptual perspective. The one strong accepting hydrogen bond of NH_3 is thought to leave the three N-H groups largely uncoordinated while in NH_4^+ all four N-H groups are hydrogen-bonded. To further quantify hydrogen bonding interactions and associated dynamics we present in Figure 1 the radial distribution functions $g(r)$ for the hydration of NH_3(aq) and NH_4^+(aq). In addition, we have decomposed the radial distribution functions $g(r)$ for N-O_w and H-O_w into individual contributions from specific hydrated N-H_i bonds assigned momentarily in order of increasing distance to the closest hydrogen bonded O_w of water. This approach allows us to study the degree of asymmetry in hydrogen bonding for formally equivalent molecular N−H bonds. We refer to Figure S1 for an accumulative coordination numbers $n(r)$ derived from the radial distribution functions $g(r)$. We complement our discussion by analyzing the hydrogen bond statistics as derived from the AIMD simulations (see Table S1 in the SI), numbers as contained in the $g(r)$ calculated according to the geometric definition as given in the SI for both R_{H-bond} = 2.5 Å as well as R_{H-bond} = 2.8 Å (and a maximum angle of 30 degrees between the vectors O-H and O-O); the criterion with elongated distance was used to evaluate the stability of the results).

From the $g(r)$ and $n(r)$ functions of N-O_w and H-O_w in Figures 1 and S1, we observe that the NH_4^+ ion shows a distinct first hydration shell with around 6 water molecules, slightly larger than previous results,[2-11] and all four N−H groups donate hydrogen bonds. The NH_3 molecule [26] on the other hand accepts a hydrogen bond from water forming a long-lived H−O−H···NH_3 complex, which appears to be stable throughout the AIMD trajectory. The accepting hydrogen bond is seen as a distinct peak in the $g(r)$ of N-H_w and gives rise to the first peak in the $g(r)$ of N-O_w, which however is overlapping with contributions from donating hydrogen bonds. The hydrogen bond donation from NH_3 to water as observed in the $g(r)$ for N-O_w or H-O_w is less well defined and without clear minima in the $g(r)$ for N-O_w or H-O_w, it is not meaningful to give a coordination number. The asymmetry in hydrogen bond acceptance and donation around the ammonia molecule is determined by the strength of hydrogen bond acceptance relative to donation from ammonia to water, which has been investigated before.[15]

The decomposition in Figure 1 of the $g(r)$ radial distribution functions for N-O_w and H-O_w allows us to further explore the possible different hydrogen bond motifs and the asymmetry on the donating side. For example, the resulting thin grey line for N−H_1 in the top left of Figure 1 is obtained from averaging over all configurations in the NH_4^+(aq) trajectory, but selecting the N−H group with the shortest hydrogen bond and then determining the $g(r)$ of N-O_w and H-O_w for the corresponding water molecule. Analogously for N−H_2, the N−H group with the second shortest H-bond is sampled, and so on. Thereby we can quantify the instantaneous asymmetry around ammonium and ammonia. We see that for NH_4^+(aq), the first three N−H groups have rather sharp peaks in the $g(r)$ of both N-O_w and H-O_w , whereas the $g(r)$ for the fourth N−H group N−H_4 has significantly broader features. The dashed grey lines in Figure 1, the distribution from the remaining water molecules, show that only N−H_4 has a tendency of bifurcation with another water molecule in the range of hydrogen bonding. For NH_3(aq), all three N − H groups have broad features in the $g(r)$ of both N-O_w and H-O_w, clearly showing the weakness of hydrogen bond donation without significant asymmetry.

The precise details of the hydration depend on the accuracy of the quantum chemical approximations, and our investigation is limited to standard DFT (BLYP) with inclusion of dispersion. Dispersion corrections have been shown to improve the description of liquid water for the BLYP.[71] From the comparison of the present simulation results in Figure 1 with the pure BLYP results from CPMD,[26] we notice only a small influence of dispersion on the hydrogen bonding around NH_3(aq) and NH_4^+(aq). However, there is an increase from 5 to 6 water molecules in the first hydration shell of NH_4^+(aq), when the dispersion corrections are introduced.

As a consequence of the differences in hydrogen bond strengths, the NH_3 and NH_4^+ species undergo substantially different dynamics. Rotational dynamics of the ammonium ion has previously been shown to be hindered by strong hydrogen bonds with the neighbouring water molecules.[2,4,10,33] Hence, the NH_4^+ ion undergoes a rotational motion characterized by discontinuous rotational jumps associated with the exchange of first hydration shell.[2] This picture is qualitatively confirmed in our present simulations. The ammonia molecule on the other hand has only one strong hydrogen bond from water to the nitrogen lone-pair. The reorientation of C_{3v} symmetry axis in NH_3 molecule is slow, since it is restrained by the motion of the long-lived H−O−H···NH_3 complex. In contrast to the ammonium ion, NH_3 has only weak donating hydrogen bonds to the nearby water molecules and as a consequence there is a nearly free rotation around C_{3v} symmetry axis of the NH_3 molecule.

In summary, the AIMD simulations show a two-fold asymmetry in the hydration of the solutes. On the one hand hydrogen bond donation (N−H···O) around the hydrated NH_3 is weak, whereas that of hydrated NH_4^+ is strong. On the other hand, while NH_3 is not involved in strong donating hydrogen bonding, it does accept a long-lived hydrogen bond from water that lasted throughout the 40 ps time span of the AIMD simulation. For the NH_3 molecule,

the results of the hydrogen bond analysis are strongly dependent on the geometric criteria used (see Table S1). Furthermore, there is a rapid exchange of hydrogen bonds of the N-H groups during rotation around the symmetry axis of NH_3. We suggest that a further quantification may well require a derivation of hydrogen bond lifetimes from hydrogen bond exchange time-correlation functions. The NH_4^+ ion, on the other hand, is predominantly (> 60% of the time) in a full hydrogen-bonded configuration with four donating hydrogen bonds to water and occasionally passes through configurations with one broken hydrogen bond.

3. FT-IR Spectroscopy of Aqueous NH_4^+ and NH_3

FT-IR spectroscopy of solutes in aqueous solution is challenging due to the strong absorption by the solvent water in large parts of the mid-infrared spectral region. This is in particular the case for the hydrogen stretching vibrations, that have been well studied due to the much reported empirical correlations between hydrogen stretching mode frequency shifts and hydrogen bond strengths.[52-57] Less trivial is the disentanglement between frequency shifts caused by specific hydrogen bond interactions and those due to couplings of the hydrogen-bonded complexes with polar solvent shell interactions, making a quantitative assessment of intrinsic hydrogen bond strengths involved.[59,61] We pursue attenuated total reflection measurements of aqueous NH_3 and NH_4Cl solutions, where we vary the concentration, and aim to determine the spectral position of the solute bands by two-dimensional correlation spectroscopy (2D-COS). In Figure 2 we show the linear FT-IR spectra measured in ATR mode of NH_3 and of NH_4^+ in aqueous solution for different solute concentrations. Particular IR-active bending modes of the solute species NH_3 and NH_4^+ in aqueous solution are directly observable because these are clearly separated from the solvent water modes. In contrast the substantial spectral overlap of N-H and O-H stretching bands prevents a direct determination of frequency position and spectral breadth of these aqueous solutes. To get more information on the bands correlation and to sort out spectrally overlapping peaks, we apply the generalized 2D correlation analysis based on the Noda concept.[72,73] In this method, the congested spectra of perturbed sample consisting of many overlapped peaks can be simplified and the spectral resolution increased by spreading peaks over a second dimension. Each type of spectral event, such as band shifting, overlapping bands of which the intensity changes in the opposite direction, band broadening, baseline change, etc., has a particular 2D pattern. The intensity of a synchronous 2D correlation peak $\Phi(\nu_1, \nu_2)$ represents simultaneous or coincidental changes of two separate spectral intensity variations measured at ν_1 and ν_2. In contrast, the intensity of an asynchronous peak $\Psi(\nu_1, \nu_2)$ represents sequential or successive instead of coincidental changes of spectral intensities. In addition, the sign of asynchronous peaks provides information on the sequential order of spectral changes. Details on the 2D correlation analysis are given in the SI. Figure 3 shows

the resulting synchronous and asynchronous 2D correlation analysis spectra. For a detailed description of the FT-IR results, the 2D-COS analysis as well as AIMD calculations of the IR-active modes (Figure S4) we refer to the SI, where we have added to our findings existing literature values of vibrational frequencies (Tables S2 and S3).

From the aqueous NH_3 measurements (Figure 2a) and 2D-COS analysis (Figure 3a,b) we conclude that: a) The symmetric ν_2 bending vibration of NH_3 is located at 1108 cm^{-1}; b) The synchronous 2D contour map (Figure 3a) is dominated by the solvent water O-H stretching and bending contributions; and c) The asynchronous 2D spectrum (Figure 3b) reveal three bands that are asynchronous to the broad O-H stretching absorption of water with maxima located at 1108 cm^{-1}, 3013 cm^{-1} and 3396 cm^{-1}. From this we derive that the bands at 3013 cm^{-1} and 3396 cm^{-1} must be due to the H−O−H···NH_3 complex. The AIMD calculations (Figure S4) show that the narrow band at 3396 cm^{-1} (FWHM ~ 40 cm^{-1}) is due to the ν_3 fundamental N-H stretching transition of NH_3, whereas the broad band at 3013 cm^{-1} has predominant contributions from the O-H stretching band of water hydrogen-bonded to the NH_3 lone pair. With this finding we unequivocally identify the location of the N-H stretching band of aqueous NH_3, as well as of the O-H stretching band of the water molecule hydrogen-bonded to the NH_3 lone pair, using the 2D-COS analysis, without any assumptions on particular hydrogen bonding equilibria,[51] thus preventing a biased outcome of the analysis caused by the choice of particular equilibrium settings.

From the aqueous NH_4^+ measurements (Figure 2b) and 2D-COS analysis (Figure 3c,d) we conclude that a) The asymmetrical deformation (bending) ν_4 mode of NH_4^+ is located at 1456 cm^{-1}; b) The synchronous 2D-COS analysis shows a direct positive correlation of the ν_4 mode with two bands located at 2896 cm^{-1} and 3068 cm^{-1} (that can thus be assigned to the $2\nu_4$ overtone and ν_1 fundamental transitions of aqueous NH_4^+); c) a negative correlation in the synchronous 2D-COS analysis exists with bands located at 3300 and 3630 cm^{-1}, that we assign to water; and d) A detailed analysis of the asynchronous 2D spectra shows that this 3300 cm^{-1} band has a markedly different behaviour than those of the neighbouring bulk water maxima at 3200 cm^{-1} and 3400 cm^{-1}, but similar to the band at around 3630 cm^{-1} (see Figures S2, S3 and associated discussion in the SI). We therefore assign the 3300 cm^{-1} and 3630 cm^{-1} bands to the O-H stretching transitions of interstitial water, with lower average number of hydrogen bonds compared to bulk water. The concentration of bulk water decreases slower (if at all) than the concentration of the interstitial water with increasing concentration of NH_4Cl (as derived from the sequential order of spectral changes based on Noda's rules, see SI). Whether these findings suggest that for NH_4^+ hydration shell water has a lower average number of intermolecular hydrogen bonds, and whether these provide insight into the coordination dynamics of NH_4^+ as found in QM/MD calculations [2-11] or that water interacting with Cl^- is responsible for this observation, remains a topic of further research.

Summarizing this part, we can conclude that NH_3(aq) does have a strong hydrogen bond between the lone pair of NH_3 and the hydrogen bond donating water molecule. The observed frequency shifts for the N-H stretching transitions (30-50 cm^{-1} downshift compared to the gas phase) hint at a minor or even negligible hydrogen bond donating capability of NH_3 to nearby solvent shell water molecules. Interestingly, only a single asymmetric N-H stretching band is observed, suggesting that any specific local hydrogen bond interaction should be shorter lived than the N-H stretching dephasing time. In contrast, the N-H stretching and bending modes of NH_4^+(aq) reflect the hydrogen bond interactions by having the N-H groups donating a hydrogen bond to the lone pairs of surrounding water molecules, in line with significant N-H stretching frequency downshifts on the order of ~ 170-200 cm^{-1}. Realizing that a direct connection between frequency shifts and hydrogen bond strengths cannot be made, as one has to distinguish between contributions by non-specific solute-solvent interactions and specific hydrogen-bond interactions, that necessitate dedicated QM/MD calculations on the vibrational dephasing and spectral diffusion dynamics,[59,61] we can at this stage state that the donating hydrogen bonds of NH_3(aq) are ultraweak, the accepting hydrogen bond with one water molecule is medium strong (using the conventional terminology of hydrogen bonds [52-57]). The hydrogen bonds of NH_4^+(aq) are of the weak hydrogen bond category. Ultimately, these steady-state FT-IR studies also show the limitations of using local vibrational modes to probe hydrogen bond properties: substantial spectral overlap with the solvent water makes a quantitative determination of intrinsic hydrogen bond strengths challenging. Many QM/MD studies on in particular water have shown that the frequency spread due to interactions with the surrounding solvent shells can be of the same order of magnitude as the intrinsic hydrogen bond frequency shift. Dedicated studies of hydrogen bonded complexes in solvents of different polarities can elucidate this issue.[74] Ultrafast infrared spectroscopy will provide additional information on the mode couplings and dynamics of hydrogen bonds. In particular the role of spectral diffusion in vibrational line shapes needs to be further explored. However, it remains a serious challenge to probe small signals of the solute underneath the strong contributions by the solvent water in the N-H/O-H stretching spectral range in these time-resolved studies. Here we follow a different route, by use of a different local probe: the N K-edge absorption of the solutes, which are more apparent as spectral overlap of the solvent water is much less restrictive. This will be discussed in the next section.

4. Soft-X-Ray Spectroscopy of Aqueous NH_3 and NH_4^+

Figure 4a shows the soft x-ray absorption spectra (XAS) measured at the N K-edge of aqueous NH_3 and NH_4^+ solutions. The XAS of NH_3 (aq) exhibits a pre-edge peak at 401.2 eV, a sharp main band at 402.8 eV and a tail due to post-edge transitions between 403 and 414 eV. For NH_4^+ a minor pre-edge peak at 403-404 eV appears as a small shoulder to the main

band located at 405.7 eV. In addition to that, a pronounced post-edge shoulder is present at 409 eV. For comparison to our experimental results we show the calculated XAS using the full core-hole excited (XFH) approximation [67,75] sampled over the AIMD trajectories (Figure 4b). To understand the role of hydrogen bonding interactions in shaping our theoretical XAS results obtained from the AIMD calculations, we inspect calculated spectra for ammonia and ammonium ion with optimized structures in the gas phase, with solution phase optimized structures without surrounding solvent forming hydrogen bonds, and for the full solvent shell case including hydrogen bonds. With this step-by-step analysis we aim to distinguish effects in the calculated XAS spectra due to structural changes from those caused by hydrogen bonding interactions.

The calculated N K-edge spectra of the geometry optimized gas-phase NH_3 and NH_4^+ species are displayed in Figure 5a,d. We find for NH_3 a considerable pre-edge transition below 401 eV and a strong main edge transition(402 eV). In contrast to NH_3, we find no pre-edge peak in NH_4^+ and only one main-edge transition (406 eV). As is demonstrated below, all other intensities at higher photon energies in both systems can be assigned to transitions in the main edge or to Rydberg and continuum states. The missing clear Rydberg structure above the main edge [63,70] and the expected missing intensity typically forming continuous intensity distributions at higher energies [70] are due to the approximations of our XFH calculations and basis sets. We thus focus our interpretation predominantly at the pre- and main-edge.

The changes in intensity of the pre-edge peaks in NH_3/NH_4^+ can be understood by inspecting the symmetries of the unoccupied orbitals reached in the XAS transitions. We can approximately assign the pre-edge peak to transitions to the lowest unoccupied molecular orbital (LUMO) whereas the main-edge peak corresponds to transitions to the LUMO+1 and higher. With C_{3v} molecular symmetry in NH_3, the LUMO (pre edge transition) has a1 symmetry with considerable N 2p character.[63] As we probe the amount of 2p character in unoccupied orbitals with N K-edge XAS within the dipole selection rule (s to p transitions) we find a pre-edge peak in NH_3. For NH_4^+ in perfect tetrahedral symmetry, the LUMO has a1 symmetry (i.e. pure 2s character without additional 2p contribution). As a consequence, similar to isoelectronic CH_4, the 1s to LUMO transition is dipole forbidden and the pre-edge peak is quenched in NH_4^+. The LUMO+1 in both NH_3 and NH_4^+ has dominant (in NH_3) or exclusive 2p character (in NH_4^+) explaining the strong main-edge peaks for both cases.

We next investigate the effect of variations in intra-molecular structures on the XAS spectra, first where NH_3 and NH_4^+ are surrounded by water molecules, but not interact with them implying no hydrogen bonds formed, and secondly - explicitly including interactions with solvent molecules. The calculated N K-edge spectra of the NH_3 and NH_4^+ structures extracted from solution are displayed in Figure 5b,e, respectively. For both species we find the same overall spectral shape as for the corresponding optimized gas-phase structures with a pre- and a main-edge peak in NH_3 and a main-edge peak in NH_4^+. Peaks apparently are

inhomogeneously broadened compared to the optimized gas-phase (visible in particular for the main edge in NH_4^+) due to shifts of the peaks on the 0.1 eV level when varying the intra-molecular structure. Interestingly, we also observe a small pre-edge intensity for NH_4^+ at around 404 eV for the solution structures in contrast to the optimized gas-phase structure. This can be explained by a "dynamical breaking" [63] of tetrahedral symmetry in the solution structure ensemble by intra-molecular deformation due to asymmetrical N-H stretching vibrations with a concomitant increase of LUMO 2p character and hence pre-edge intensity increase as compared to the optimized gas-phase structure. In addition, the main-edge energy in NH_4^+ is found to slightly red-shift by about 0.2 eV upon distortion in the solution structure ensemble (most likely the N-H elongations) compared to the optimized gas-phase case.

Finally, in Figure 5c,f we compare the N K-edge spectra of NH_3 and NH_4^+ in solution as calculated for the ensembles of structures from our MD simulations hence now including explicit interactions with solvent molecules. In contrast to the optimized gas-phase and to the solution structures without solvent we find that the spectra of both systems in solution are considerably broadened with main-edge bands (instead of peaks) of approximately 3 eV FWHM with sharp rising edges and considerable asymmetry towards higher energies. We interpret the results as following: solute-solvent interactions, including hydrogen bonding, cause the main-edge peaks of the individual solute molecules to shift or to split on the level of several eV due to interactions with the surrounding water molecules hence forming the observed main-edge bands in the solution ensembles. In addition, the solution calculations now also exhibit a clear edge jump with step-like increases of absorption continuously extending all the way to the maximum displayed incident energy of 418 eV. This in addition points to the formation of continua of unoccupied states (bands) due to solute-solvent interactions. We note that for NH_3 the calculated pre- and main edges in solution are blue shifted by more than 0.5 eV relative to the isolated case. This finding is in line with the reported measured shifts of gas-phase and solvated NH_3 pre- and main edges,[26] indicating the potential of establishing correlations between solute-solvent interactions and a spectral feature. The pre-edge intensity of NH_4^+ in aqueous solution is further increased to a clear peak or shoulder at 403-404 eV in the solution spectrum apparently directly indicating the impact of the solute-solvent interactions. The main-edge transitions show a further red-shift in solution by about 0.1-0.2 eV compared to the isolated case in NH_4^+, suggesting a potential correlation with hydrogen bonding may exist.

Figure 4b shows a comparison of the measured and calculated spectra of NH_3 and NH_4^+ in aqueous solution. The frequency offset of the calculated spectra were matched to the experimental ones. We can see a good agreement in the pre-edge and main-edge spectral features for both species. This justifies a more detailed analysis of the nature of the solute-solvent interactions in general and the associated hydrogen bonding interactions in particular. For this we follow the systematics discussed with Figure 5 and inspect in detail

the molecular orbitals reached upon 1s excitation in the pre-, main- and post-edge transitions with the orbital plots, as shown in Figure 6.

We find the molecular orbital reached upon pre-edge excitation in NH_3 in water (Figure 6 c) to be similar to the LUMO (a_1) of gas-phase NH_3. As in the gas phase, it is an N-H anti-bonding orbital localized along the N-H groups with large amplitudes at the H atoms. The intensity of the pre-edge peak in NH_3 in solution (also in the presence of the strong accepting hydrogen bond) is hence as in the gas phase due to the intrinsic deviation from tetrahedral symmetry in NH_3. Furthermore, for NH_3 in solution, the pre-edge intensity is found to increase with increasing H-bond distance: The larger the cavity on the N-H side, the more intense is the pre-edge peak. This relation is similar to the case of the pre-edge peak in the water molecule in water solution and can be explained by increasing 2p character upon lengthening the distance to the surrounding water.[62] By comparison to the isolated cases in Figure 5 and in agreement with results by Weinhardt *et al.* [26] we find the energy of the pre-edge in NH_3 in solution to be primarily determined by the accepting hydrogen bond on the N lone-pair side of NH_3. This is consistent with the earlier observation in Weinhardt *et al.*, where the measured gas-phase pre-edge energy was reproduced in a calculation when the H_2O molecule on the hydrogen bond accepting side of NH_3 had been instantaneously removed from the solution. The corresponding pre-edge blue shift upon solvation was explained by electrostatic interaction with surrounding water molecules.[26] Here we find the pre-edge peak in NH_3 in solution to be due to a single transition. In a ground-state (no core hole) density-of-states picture this corresponds to saying that the pre-edge orbital energy resides in the band gap of water without interactions with the molecular orbitals of water (no energy dispersion due to mixing with water density of states). Evaluating the sampled spectra for NH_3 (aq), we notice a clear correlation between hydrogen bond asymmetry and pre-edge energy: The shorter the accepting hydrogen bond of NH_3(aq) on the N lone-pair side the larger the pre-edge energy. This correlation has the same origin as the blue shift of the gas-phase NH_3 pre-edge peak upon solvation.

As for NH_3, we also find that pre-edge excitations for isolated NH_4^+ as well as for NH_4^+ in solution can be assigned to transitions to a single molecular orbital of similar a_1 symmetry with concomitantly dominant 2s character) for isolated NH_4^+ as well as for NH_4^+ in solution. The intensity of the pre-edge peak in NH_4^+ in solution therefore is, like in the isolated case, predominantly due to intramolecular symmetry distortions, and the larger the distortion the higher the pre-edge intensity. The pre-edge intensity is in addition a measure of the asymmetry in hydrogen bonding, as the NH_4^+ a_1 LUMO is further distorted through hybridization with surrounding water $3a_1$ orbitals in the strong donating hydrogen bonds of NH_4^+. The intra-molecular asymmetry seems to dominate over the inter-molecular asymmetry, but the pre-edge feature in NH_4^+ (aq) is too weak to investigate the effect in detail.

The main-edge peak in NH_3 in solution can be traced back with our calculations to transitions to two N-H anti-bonding orbitals of e symmetry where one is displayed in Figure 6b. They have large amplitudes at the H atoms in NH_3 and therefore exhibit a similar blue-shift upon solvation as the pre-edge transitions. They are also found to be slightly anti-bonding in the hydrogen bond donation direction involving a weak hybridization with the occupied water $3a_1$ orbital. We note that the corresponding energy level is degenerate in isolated NH_3 whereas it is split by the asymmetry in the solute-solvent interactions in NH_3 in solution. The splitting due to asymmetry together with dispersion due to hybridization with water orbitals explain the large width of the main-edge band in NH_3 in solution compared to the sharper main-edge peak in isolated NH_3. For NH_4^+ we find the main-edge transitions correspond to unoccupied orbitals which have t_2 symmetry for the perfectly tetrahedral NH_4^+ ion (Figure 6e). The shape of these orbitals is similar to the orbitals reached upon main-edge excitation NH_3 (Figure 6b) with the marked difference in NH_4^+ that they considerably overlap and hybridize with the H_2O $2b_2$ orbitals of those water molecules involved in the donating hydrogen bonds of NH_4^+. For neither NH_3 nor NH_4^+ in solution we find a clear correlation of the main-edge energy or intensity with hydrogen bond asymmetry or coordination.

Two selected molecular orbitals for excitations in the post-edge regions of NH_3 and NH_4^+ in solution are displayed in Figure 6a,d. As for these two we found most unoccupied orbitals for post-edge transitions to be much more delocalized to the surrounding water molecules through hybridization with H_2O orbitals compared to the orbitals for the pre- and main-edge transitions. This indicates a particularly strong sensitivity of the post-edge transition energies to variations in intra- and intermolecular structure. With the large continuum-like distribution of distances and angles in the structures from the MD simulation this explains the structure-less and continuum-like intensity distribution following in the post-edge regions. We note that the apparent broad post-edge peak in the measured spectrum of NH_4^+ in solution at around 408-410 eV is not reproduced in our calculations, due to limitations of the XFH method.

5. Electronic Structure of Aqueous NH_4^+ and NH_3

For further analysis of the simulated XA spectra, we investigated the electronic structure of the NH_3(aq) and NH_4^+(aq) solutions, by sampling the partial density of states (PDOS) over the same configurations as used for the XA spectra.

In the left panel of Figure 7, the O2*p* and N2*p* PDOS of the occupied Kohn-Sham orbitals are presented. Since a majority of the water molecules have an aqueous environment, the O2*p* PDOS of NH_3(aq) and NH_4^+(aq) solutions are in close agreement with each other and also with the electronic structure of pure liquid water [76] as observed in previous AIMD

simulations and photoelectron spectra. At the edge of the valence band in water (at low binding energies around 6-7 eV), there is the signature of the water lone-pair orbital, denoted $H_2O(1b_1)$ in the C_{2v} point group symmetry. The bonding water orbitals are observed at 8-10 eV [$H_2O(3a_1)$] and 11-13 eV [$H_2O(1b_2)$]. Hydrogen bonding in liquid water is known to primarily give rise to a broadening in the 8-10 eV region due to the large overlap and hybridisation of $H_2O(3a_1)$ orbitals on neighbouring water molecules.[76]

In contrast to the solvent, the protonation of the solute has a profound influence on the N2*p* PDOS of occupied orbitals as seen in the comparison of the coloured curves in the left panel of Figure 7. The NH_3 molecule has two occupied orbitals with strong N2*p* character in the region around 11 eV [a bonding orbital denoted $NH_3(1e)$] and a non-bonding lone-pair orbital around 6 eV [denoted $NH_3(3a_1)$]. The $NH_3(1e)$ levels occurs in between the PDOS features of water and whereas the $NH_3(3a_1)$ level partially matches the $H_2O(1b_1)$ level energetically, in both cases without significant geometric overlap between the solute and solvent orbitals. In between, there are again the signatures of hybridisation due to hydrogen bonding as carefully investigated in the previous RIXS study.[26] The NH_4^+ ion has four equivalent N-H σ bonds resulting in a strong feature [originating from the gas phase $NH_4^+(1t_2)$ orbitals] in the N2*p* PDOS around 11-13 eV overlapping perfectly with the $H_2O(1b_2)$ levels. Similarly to liquid water,[76] however, the dispersion in this feature is due to variations in the N-H bond lengths rather than to hybridisation related to hydrogen bonding. Instead, the hydrogen bonding of the hydrated NH_4^+ ion shows up as weak features in the regions of [$H_2O(3a_1)$] and [$H_2O(1b_2)$]. For both solutes, we note the signatures at 9 eV and at 6.5 eV in the solute N2*p* PDOS from a weak hybridization with the bonding $H_2O(3a_1)$ and non-bonding $H_2O(1b_1)$ orbitals. In conclusion from the analysis of the occupied PDOS, we stress the differences in the orbital hybridization in the hydrogen bonding between water molecules and in the hydrogen bonding of the hydrated solutes. Here a clearly different picture emerges for hydrogen bonding of NH_4^+/NH_3 in water, compared to the hydrogen bonding between water molecules. Regardless of the protonation state, the NH_4^+/NH_3 PDOS do not match energetically with the $H_2O(3a_1)$ levels, and – thus – hydrogen bonding of NH_4^+/NH_3 to water occurs without significant orbital overlap, and associated substantial charge transfer.

In the right panel of Figure 7, we have investigated the electronic relaxation of the unoccupied orbitals in the different approximations to simulate XA spectra based on the transition potential method with varying occupation in the N1*s*(α spin) orbital from a full core-ionized state (FH XAS), a half-a-core-hole model (HH XAS) and a ground state calculation (GS - no core-hole). In each case, the spectra are calculated as orbital transitions. The spectra are aligned with the total density of states (unoccupied orbitals) which resemble the O2*p* PDOS. In the latter case (GS), the unoccupied Kohn-Sham orbitals are determined from the same ground state calculation as the occupied PDOS presented in in the left panel of Figure 8. The comparison shows that the sharp main-edge feature in each of the XA spectra of NH_3(aq) and NH_4^+(aq) gradually form with decreasing core-hole occupation.

However, the relative shift in the main-edge in the N K-edge spectra due to protonation is present already for the ground state (GS XAS) calculations, and persists in the electronic relaxation related to the inclusion of the core-hole, which is a final state effect. Hence, the relative shift of the XA spectra of NH_3(aq) and NH_4^+(aq) is an initial state effect directly related to the hydration (thus, the difference in hydrogen bonding) and is not an effect of the spectroscopic probe.

Furthermore, from the alignment of the XA spectra against the O2*p* PDOS, we can explain how come the shape of the XA profile changes so dramatically with the degree of occupation in the core-hole; from the broad shape of the GS XAS to the sharpness of the FH spectra. Due to the electronic relaxation, giving a screening in the presence of the core-hole, the orbital mixing between the solute orbitals and the orbitals of the surrounding hydration shell is reduced. The N-H anti-bonding orbitals are pulled down towards the band gap of liquid water for the HH and FH approximations. For NH_3(aq), the N-H groups are only involved in clearly weak hydrogen bonding interactions with nearby water molecules, and there are XA spectra at the water conduction band edge already in the ground state configuration. The N-edge XA intensity primarily arise from the N2p character in the unoccupied states, which can be associated with the anti-bonding NH_3(2e) orbitals. Hence, in the presence of the core-hole the N-H anti-bonding orbitals are placed deeply into the band-gap region. For NH_4^+(aq) on the other hand, it is only for the FH approximation that the N-H anti-bonding orbitals approaches the band gap giving reduced broadening of the XA spectrum of the NH_4^+ ion.

Thereby, using the combination of x-ray spectroscopy and spectrum simulations, we can extend the understanding of the hydrogen bonding around the solutes in NH_4^+(aq) and NH_3(aq) and connect the structural descriptors from AIMD simulations and IR spectroscopy to the nature of electronic structure in the hydrogen bonding.

6- Conclusions

Using a combined approach of ab initio molecular dynamics (AIMD) calculations, and experimental IR and N K-edge spectroscopy as local probes for hydrogen bonding, we characterise the hydration structure and associated dynamics of NH_3(aq) and of NH_4^+(aq). NH_3(aq) has one medium strong hydrogen bond with water through its lone pair. The N-H donating side of NH_3(aq) on the other hand has ultraweak – if at all – hydrogen bonds with the solvent water. NH_4^+(aq) has four donating hydrogen bonds to water of the so-called weak hydrogen bond category. We identify the N-H stretching (and O-H stretching) frequencies with attenuated total reflection (ATR) spectra and two-dimensional correlation spectra (2D-COS) for NH_3(aq) and of NH_4^+(aq), providing experimental confirmation of the hydrogen bond picture as indicated by the AIMD calculations. With soft-x-ray spectroscopy we measure the N K-edge spectra of NH_3(aq) and NH_4^+(aq). We are able to assess the role of

hydrogen bonding in spectral frequency shifts and broadening of the pre-edge, main edge and post edge transitions of aqueous NH_3 and NH_4^+. We calculate from a partial density of states (PDOS) analysis of bound and unoccupied orbitals for NH_3(aq) and NH_4^+(aq) that – instead of what has been derived for bulk water –orbital mixing does not occur for the bound states, and hence no significant charge transfer takes place in the hydrogen bonding interactions of NH_3(aq) or NH_4^+(aq) to the solvent water. Our findings on NH_3(aq) and NH_4^+(aq) benchmark the hydration properties of related alkylamines and alkylammonium salts.

Supporting Information

Details on Experiments and Calculations; Accumulative Coordination Numbers from AIMD Calculations; 2D Correlation Spectroscopy Analysis of FT-IR Spectra; Calculated IR Spectra; Band Assignments - Comparison to FT-IR Spectra of NH_4^+ and NH_3 in Other Media and Literature

Acknowledgement

E.T.J.N. acknowledges support from the German Science Foundation (Project Nr. DFG - NI 492/11-1). M.O. acknowledges support from the Swedish Research Council (VR contract number 2015-03956) and the Helmholtz Virtual Institute VI419 ‘‘Dynamic Pathways in Multidimensional Landscapes’’. The calculations were performed on resources provided by the Swedish National Infrastructure for Computing (SNIC). We greatly acknowledge the support of the BESSYII staff during x-ray measurements at the UE52_SGM Undulator SGM variable polarisation beamline of the Helmholtz-Zentrum Berlin and we thank Helmholtz-Zentrum Berlin for the allocation of synchrotron radiation beamtime.

References

(1) Galloway, J. N.; Townsend, A. R.; Erisman, J. W.; Bekunda, M.; Cai, Z.; Freney, J. R.; Martinelli, L. A.; Seitzinger, S. P.; Sutton, M. A. *Science* **2008**, *320*, 889.

(2) Brugé, F.; Bernasconi, M.; Parrinello, M. *J. Am. Chem. Soc.* **1999**, *121*, 10883.

(3) Liu, Y.; Tuckerman, M. E. *J. Phys. Chem. B* **2001**, *105*, 6598.

(4) Chang, T.-M.; Dang, L. X. *J. Chem. Phys.* **2003**, *118*, 8813.

(5) Zhao, Y.-L.; Meot-Ner (Mautner), M.; Gonzalez, C. *J. Phys. Chem. A* **2009**, *113*, 2967.

(6) Pattanayak, S. K.; Chowdhuri, S. *J. Mol. Liq.* **2013**, *186*, 98.

(7) Vallet, V.; Masella, M. *Chem. Phys. Lett.* **2015**, *618*, 168.

(8) Brugé, F.; Bernasconi, M.; Parrinello, M. *J. Chem. Phys.* **1999**, *110*, 4734.

(9) Pickard IV, F. C.; Dunn, M. E.; Shields, G. C. *J. Phys. Chem. A* **2005**, *109*, 4905.

(10) Intharathep, P.; Tongraar, A.; Sagarik, K. *J. Comput. Chem.* **2005**, *26*, 1329.

(11) Hesske, H.; Gloe, K. *J. Phys. Chem. A* **2007**, *111*, 9848.

(12) Kuma, S.; Slipchenko, M. N.; Momose, T.; Vilesov, A. F. *Chem. Phys. Lett.* **2007**, *439*, 265.

(13) Sälli, E.; Salmi, T.; Halonen, L. *J. Phys. Chem. A* **2011**, *115*, 11594.

(14) Mackeprang, K.; Hänninen, V.; Halonen, L.; Kjaergaard, H. G. *J. Chem. Phys.* **2015**, *142*, 094304.

(15) Orabi, E. A.; Lamoureux, G. *J. Chem. Theory Comput.* **2013**, *9*, 2035.

(16) Narten, A. H. *J. Chem. Phys.* **1968**, *49*, 1692.

(17) Narten, A. H. *J. Chem. Phys.* **1977**, *66*, 3117.

(18) Páinkás, G.; Radnai, T.; Szász, G. I.; Heinzinger, K. *J. Chem. Phys.* **1981**, *74*, 3522.

(19) Ricci, M. A.; Nardone, M.; Ricci, F. P.; Andreani, C.; Soper, A. K. *J. Chem. Phys.* **1995**, *102*, 7650.

(20) Thompson, H.; Wasse, J. C.; Skipper, N. T.; Hayama, S.; Bowron, D. T.; Soper, A. K. *J. Am. Chem. Soc.* **2003**, *125*, 2572.

(21) Slipchenko, M. N.; Sartakov, B. G.; Vilesov, A. F.; Xantheas, S. S. *J. Phys. Chem. A* **2007**, *111*, 7460.

(22) Slipchenko, M. N.; Sartakov, B. G.; Vilesov, A. F. *J. Chem. Phys.* **2008**, *128*.

(23) Katada, M.; Shishido, R.; Fujii, A. *Phys. Chem. Chem. Phys.* **2014**, *16*, 7595.

(24) Ferrario, M.; Haughney, M.; McDonald, I. R.; Klein, M. L. *J. Chem. Phys.* **1990**, *93*, 5156.

(25) Rzepkowska, J.; Uras, N.; Sadlej, J.; Buch, V. *J. Phys. Chem. A* **2002**, *106*, 1790.

(26) Weinhardt, L.; Ertan, E.; Iannuzzi, M.; Weigand, M.; Fuchs, O.; Bär, M.; Blum, M.; Denlinger, J. D.; Yang, W.; Umbach, E.; Odelius, M.; Heske, C. *Phys. Chem. Chem. Phys.* **2015**, *17*, 27145.

(27) Boese, A. D.; Chandra, A.; Martin, J. M. L.; Marx, D. *J. Chem. Phys.* **2003**, *119*, 5965.

(28) Tassaing, T.; Soetens, J.-C.; Vyalov, I.; Kiselev, M.; Idrissi, A. *J. Chem. Phys.* **2010**, *133*, 214505.

(29) Pauling, L. *The Nature of The Chemical Bond and the Structure of Molecules and Crystals*; Cornell University Press: Ithaca, New York, 1960.

(30) Pimentel, G. C.; McClellan, A. L. *The hydrogen bond*; W. H. Freeman and Co.: San Francisco, 1960.
(31) Jeffrey, G. A. *Introduction to hydrogen bonding*; Oxford University Press: Oxford, 1997.
(32) Nelson Jr., D. D.; Fraser, G. T.; Klemperer, W. *Science* **1987**, *238*, 1670.
(33) Perrin, C. L.; Gipe, R. K. *J. Am. Chem. Soc.* **1986**, *108*, 1088.
(34) Perrin, C. L.; Gipe, R. K. *Science* **1987**, *238*, 1393.
(35) Diken, E. G.; Hammer, N. I.; Johnson, M. A.; Christie, R. A.; Jordan, K. D. *J. Chem. Phys.* **2005**, *123*, 164309.
(36) Karthikeyan, S.; Singh, J. N.; Park, M.; Kumar, R.; Kim, K. S. *J. Chem. Phys.* **2008**, *128*.
(37) Karthikeyan, S.; Singh, N. J.; Kim, K. S. *J. Phys. Chem. A* **2008**, *112*, 6527.
(38) Douady, J.; Calvo, F.; Spiegelman, F. *J. Chem. Phys.* **2008**, *129*, 154305.
(39) Hvelplund, P.; Kurten, T.; Stochkel, K.; Ryding, M. J.; Nielsen, S. B.; Uggerud, E. *J. Phys. Chem. A* **2010**, *114*, 7301.
(40) Johnson, C. J.; Johnson, M. A. *J. Phys. Chem. A* **2013**, *117*, 13265.
(41) Bromberg, A.; Kimel, S.; Ron, A. *Chem. Phys. Lett.* **1977**, *46*, 262.
(42) Bertie, J. E.; Morrison, M. M. *J. Chem. Phys.* **1980**, *73*, 4832.
(43) Bertie, J. E.; Devlin, J. P. *J. Chem. Phys.* **1983**, *78*, 6203.
(44) Bertie, J. E.; Shehata, M. R. *J. Chem. Phys.* **1984**, *81*, 27.
(45) Nelander, B.; Nord, L. *J. Phys. Chem.* **1982**, *86*, 4375.
(46) Engdahl, A.; Nelander, B. *J. Chem. Phys.* **1989**, *91*, 6604.
(47) Yeo, G. A.; Ford, T. A. *Spectrochim. Act. A* **1991**, *47*, 485.
(48) Holt, J. S.; Sadoskas, D.; Pursell, C. J. *J. Chem. Phys.* **2004**, *120*, 7153.
(49) Jacox, M. E.; Thompson, W. E. *J. Mol. Spectrosc.* **2004**, *228*, 414.
(50) Jacox, M. E.; Thompson, W. E. *Phys. Chem. Chem. Phys.* **2005**, *7*, 768.
(51) Max, J.-J.; Chapados, C. *J. Mol. Struct.* **2013**, *1046*, 124.
(52) Novak, A. *Structure and Bonding (Berlin)* **1974**, *18*, 177.
(53) Lautié, A.; Froment, F.; Novak, A. *Spectrosc. Lett.* **1976**, *9*, 289.
(54) Hadži, D.; Bratos, S. In *The hydrogen bond: Recent developments in theory and experiments*; Schuster, P., Zundel, G., Sandorfy, C., Eds.; North Holland: Amsterdam, the Netherlands, 1976; Vol. II. Structure and Spectroscopy, p 565.
(55) Mikenda, W. *J. Mol. Struct.* **1986**, *147*, 1.
(56) Mikenda, W.; Steinböck, S. *J. Mol. Struct.* **1996**, *384*, 159.
(57) Libowitzky, E. *Monatsh. Chem.* **1999**, *130*, 1047.
(58) Nibbering, E. T. J.; Elsaesser, T. *Chem. Rev.* **2004**, *104*, 1887
(59) Skinner, J. L.; Auer, B. M.; Lin, Y. S. *Adv. Chem. Phys.* **2009**, *142*, 59.
(60) Bakker, H. J.; Skinner, J. L. *Chem. Rev.* **2010**, *110*, 1498.
(61) Laage, D.; Stirnemann, G.; Sterpone, F.; Rey, R.; Hynes, J. T. *Annu. Rev. Phys. Chem.* **2011**, *62*, 395.
(62) Wernet, P.; Nordlund, D.; Bergmann, U.; Cavalleri, M.; Odelius, M.; Ogasawara, H.; Näslund, L. Å.; Hirsch, T. K.; Ojamäe, L.; Glatzel, P.; Pettersson, L. G. M.; Nilsson, A. *Science* **2004**, *304*, 995.
(63) Nilsson, A.; Nordlund, D.; Waluyo, I.; Huang, N.; Ogasawara, H.; Kaya, S.; Bergmann, U.; Näslund, L.-Å.; Öström, H.; Wernet, P.; Andersson, K. J.; Schiros, T.; Pettersson, L. G. M. *J. Electron. Spectrosc. Relat. Phenom.* **2010**, *177*, 99.

(64) Sellberg, J. A.; McQueen, T. A.; Laksmono, H.; Schreck, S.; Beye, M.; DePonte, D. P.; Kennedy, B.; Nordlund, D.; Sierra, R. G.; Schlesinger, D.; Tokushima, T.; Zhovtobriukh, I.; Eckert, S.; Segtnan, V. H.; Ogasawara, H.; Kubicek, K.; Techert, S.; Bergmann, U.; Dakovski, G. L.; Schlotter, W. F.; Harada, Y.; Bogan, M. J.; Wernet, P.; Föhlisch, A.; Pettersson, L. G. M.; Nilsson, A. *J. Chem. Phys.* **2015**, *142*, 044505.

(65) Fransson, T.; Harada, Y.; Kosugi, N.; Besley, N. A.; Winter, B.; Rehr, J. J.; Pettersson, L. G. M.; Nilsson, A. *Chem. Rev.* **2016**, *116*, 7551.

(66) Yamanaka, T.; Tabayashi, K.; Takahashi, O.; Tanaka, K.; Namatame, H.; Taniguchi, M. *J. Chem. Phys.* **2012**, *136*, 014308.

(67) Hutter, J.; Iannuzzi, M.; Schiffmann, F.; VandeVondele, J. *Wiley Interdiscip. Rev. Comput. Mol. Sci.* **2014**, *4*, 15.

(68) Parent, P.; Bournel, F.; Lasne, J.; Lacombe, S.; Strazzulla, G.; Gardonio, S.; Lizzit, S.; Kappler, J.-P.; Joly, L.; Laffon, C.; Carniato, S. *J. Chem. Phys.* **2009**, *131*, 154308.

(69) Ozawa, K.; Hasegawa, T.; Edamoto, K.; Takahashi, K.; Kamada, M. *J. Phys. Chem. B* **2002**, *106*, 9380.

(70) Stöhr, J. *NEXAFS Spectroscopy*; Springer: Berlin, 1996; Vol. 25.

(71) Schmidt, J.; VandeVondele, J.; Kuo, I. F. W.; Sebastiani, D.; Siepmann, J. I.; Hutter, J.; Mundy, C. J. *J. Phys. Chem. B* **2009**, *113*, 11959.

(72) Noda, I. *Appl. Spectrosc.* **1993**, *47*, 1329.

(73) Noda, I.; Ozaki, Y. *Two-Dimensional Correlation Spectroscopy: Applications in Vibrational and Optical Spectroscopy*; John Wiley & Sons: Chicester, 2004.

(74) Psciuk, B. T.; Prémont-Schwarz, M.; Koeppe, B.; Keinan, S.; Xiao, D.; Nibbering, E. T. J.; Batista, V. S. *J. Phys. Chem. A* **2015**, *119*, 4800.

(75) Iannuzzi, M.; Hutter, J. *Phys. Chem. Chem. Phys.* **2007**, *9*, 1599.

(76) Nordlund, D.; Odelius, M.; Bluhm, H.; Ogasawara, H.; Pettersson, L. G. M.; Nilsson, A. *Chem. Phys. Lett.* **2008**, *460*, 86.

Figure 1: Hydrogen bonding configurations of NH_3(aq) (red lines) and NH_4^+(aq) are shown in snapshot pictures (top). Solute-solvent radial distribution functions of NH_3(aq) (red lines) and NH_4^+(aq) (blue lines) sampled from the present AIMD simulations are shown in the left and right panels. The radial distribution functions are presented here without the y-axis scale, since they are off-set vertically. (For proper scaling see the radial distribution functions presented in Figure S1 in the SI). Distributions of all the combinations of atomic sites (N-O_w H-O_w N-H_w H-H_w) are presented here, including, a comparison to previous AIMD simulations (dashed lines) employed for the analysis of resonant inelastic x-ray scatting of NH_3(aq) .[26]

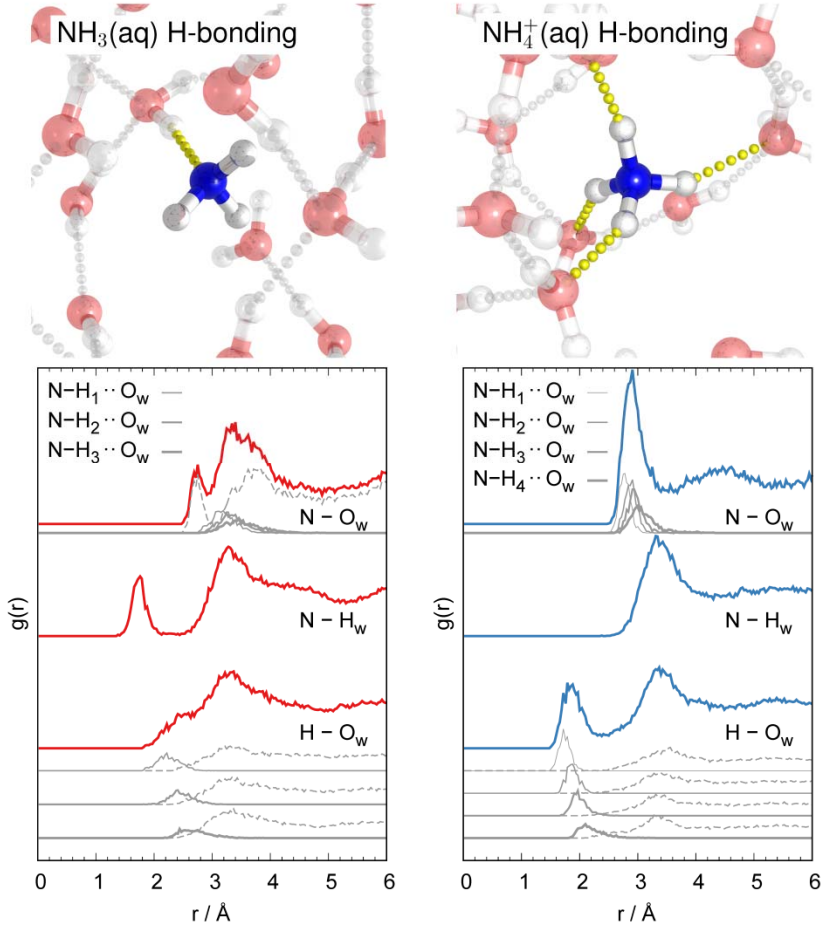

Figure 2: FT-IR spectra measured in ATR geometry for NH_4^+ and NH_3 dissolved in water at different concentrations.

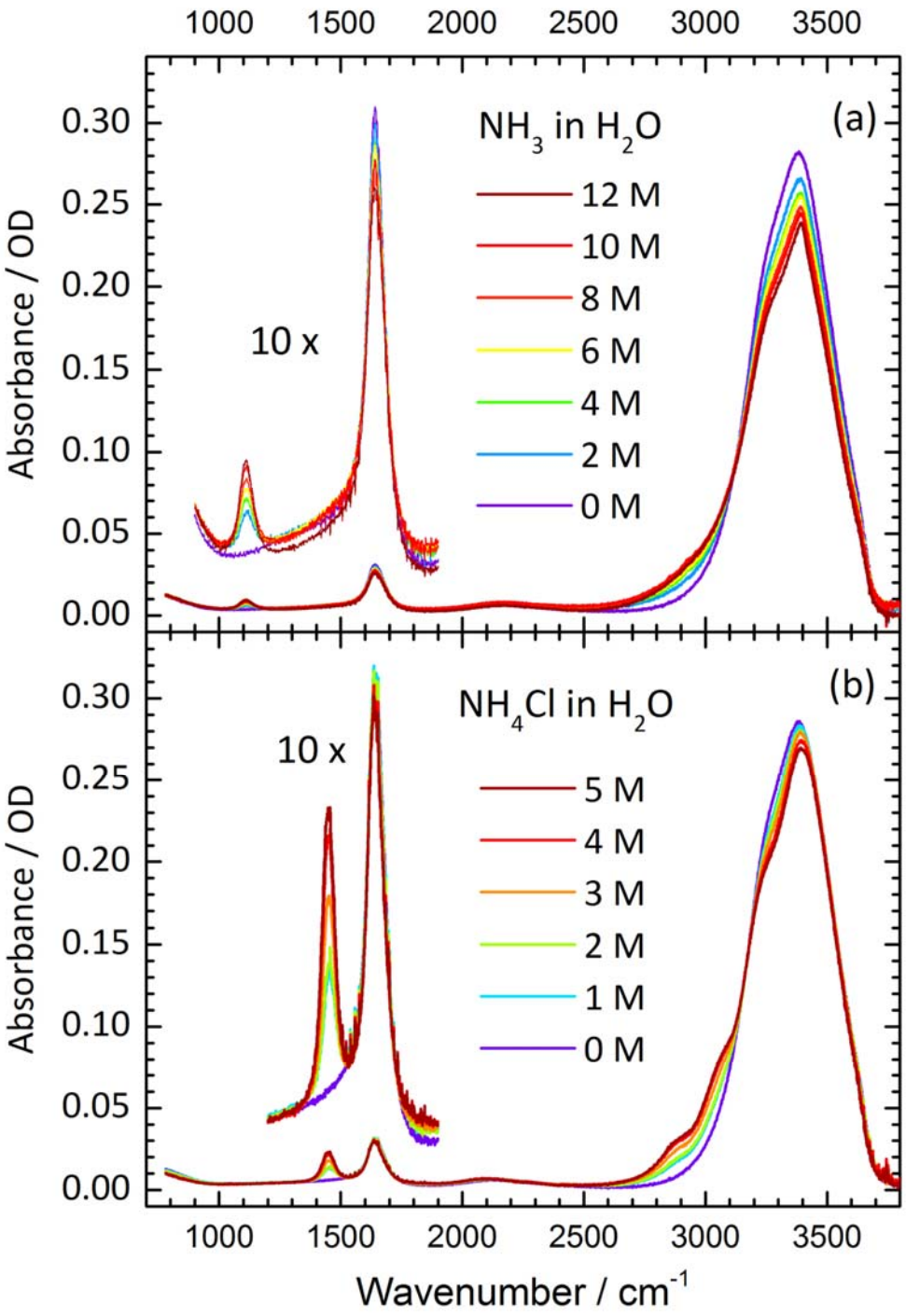

Figure 3: (a) Synchronous and (b) asynchronous 2D correlation spectra of aqueous NH_3, showing the connectivity between the water molecule O-H stretching mode strongly hydrogen-bonded to the NH_3 lone pair. The asynchronous spectrum (multiplied by the sign of the corresponding synchronous spectrum) reveal the location of the N-H stretching band of aqueous NH_3. (c) Synchronous and (d) asynchronous 2D correlation spectra of aqueous NH_4^+ reveal a band at 3300 cm^{-1}, completely hidden in 1D IR spectrum by the strong bulk water absorption. The analysis of the corresponding asynchronous spectrum (multiplied by the sign of the synchronous spectrum) allow for the assignment of the bands at 3300 cm^{-1} and 3630 cm^{-1} to the O-H stretching mode of non-bulk water entities of lower average number of hydrogen bonds.

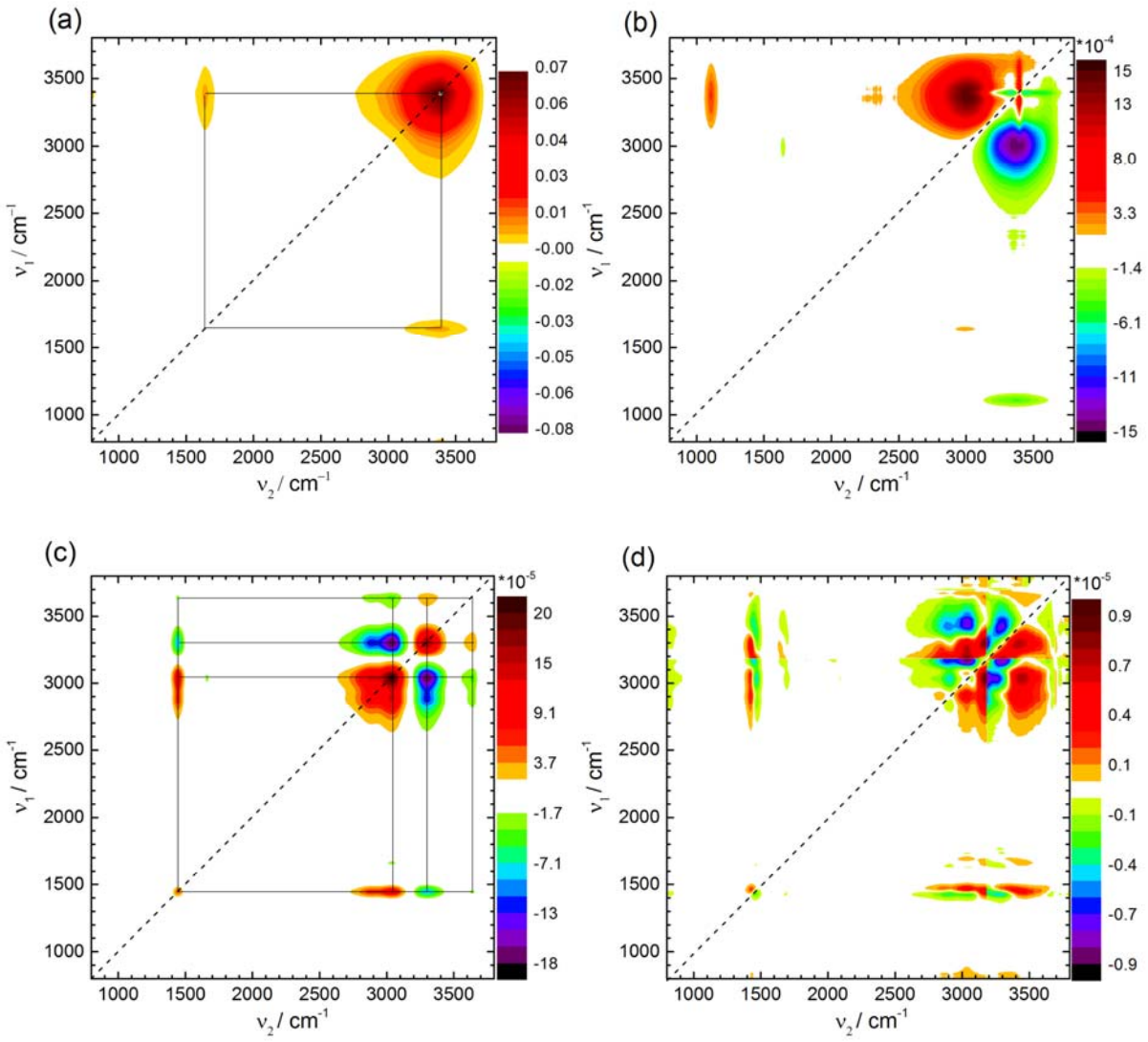

Figure 4: Simulated N K-edge X-ray absorption (XA) spectra of NH_3(aq) (red lines) and of NH_4^+(aq) (blue lines) sampled from the present AIMD simulations are compared to experimental spectra. Spectra have been calculated with the full-core-excitation (XFH) transition potential approximations.[75]

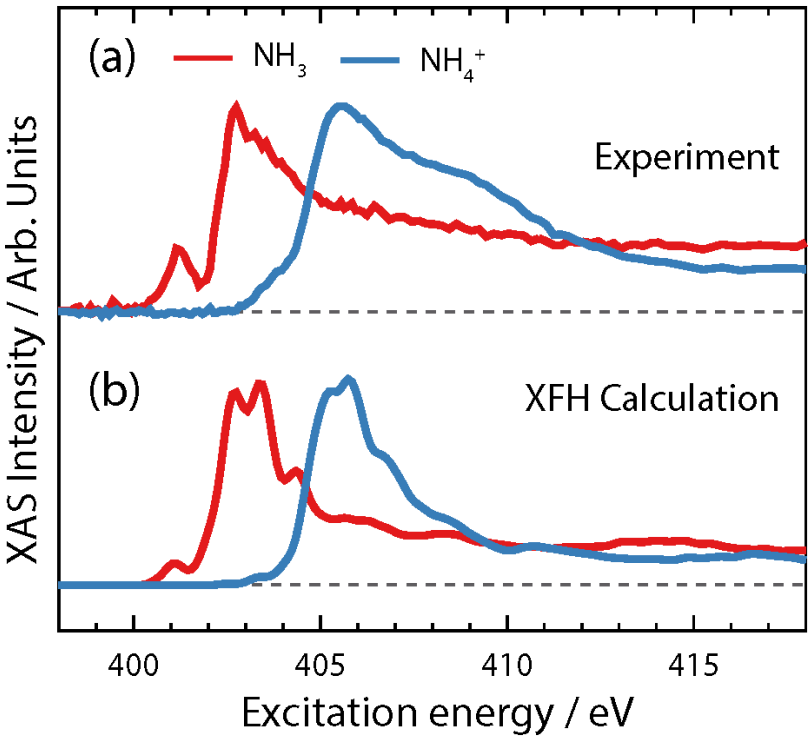

Figure 5: Simulated N K-edge X-ray absorption (XA) spectra of NH_3 (red lines) and of NH_4^+(blue lines) calculated for gas-phase equilibrium (a,d) and solution phase (c,e) structures, as well as sampled from the AIMD simulations (c,f). Spectra have been calculated with the full-core-excitation (XFH) transition potential approximations.[75]

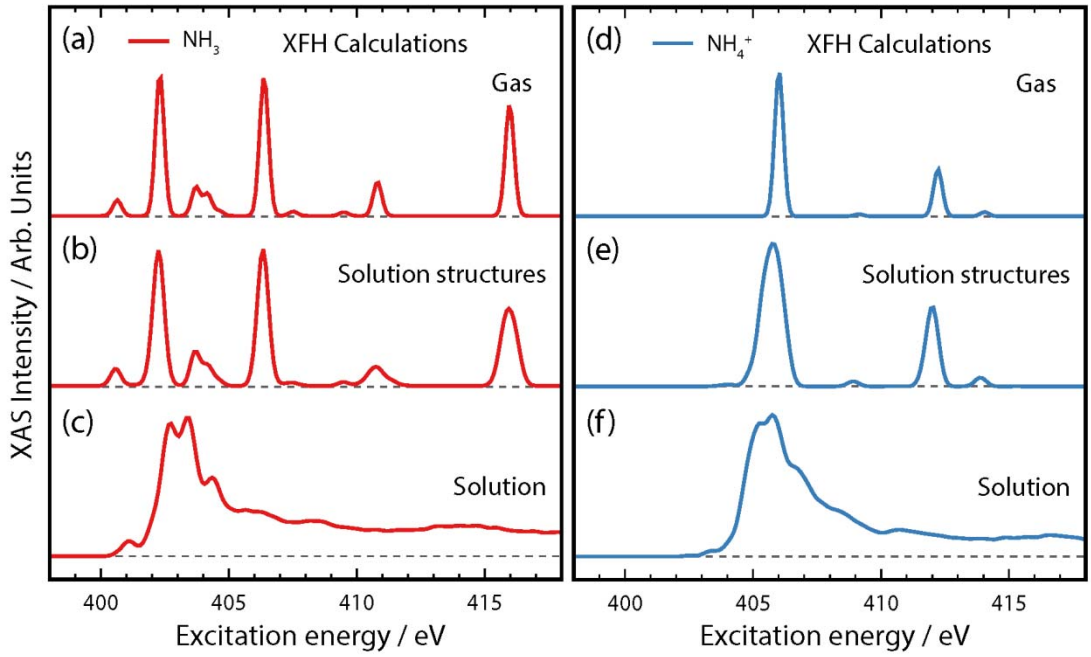

Figure 6: Unoccupied orbitals reached with the pre-edge main edge and post-edge N 1s excitations. The orbitals are taken from XFH calculations [75] of $NH_3(H_2O)_4$ and $NH_4^+(H_2O)_4$ clusters. The solutes are oriented with the C_3 symmetry axis vertical in the plane of the pictures.

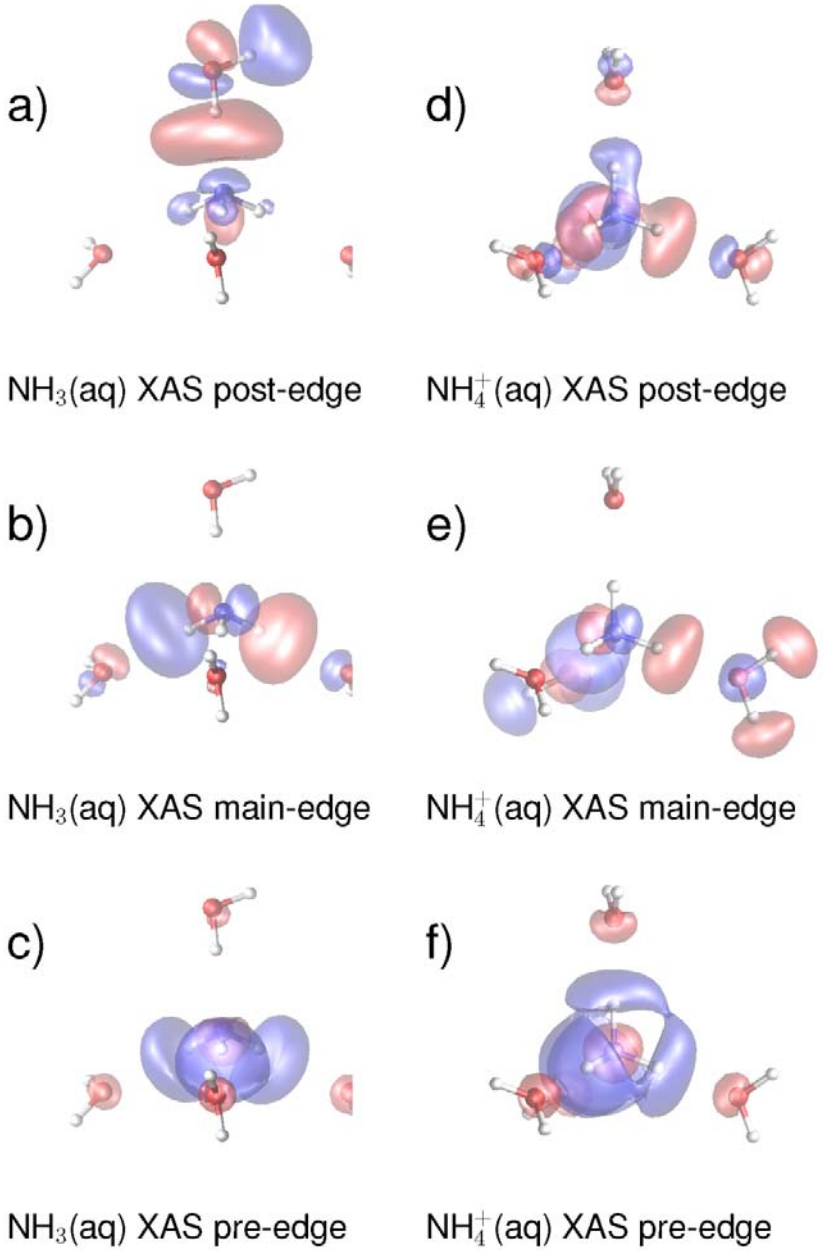

Figure 7: Partial density of states (PDOS) on nitrogen and oxygen in NH_3(aq) (red lines) and NH_4^+(aq) (blue lines) sampled from the present AIMD simulations. Left panel: occupied p-PDOS of nitrogen and oxygen. Right panel: Simulated N K-edge XA in the half-core-hole (HH) and full-core-hole (FH) transition potential method align for the HH NH3(aq) calculation against the GS unoccupied p-PDOS of oxygen.

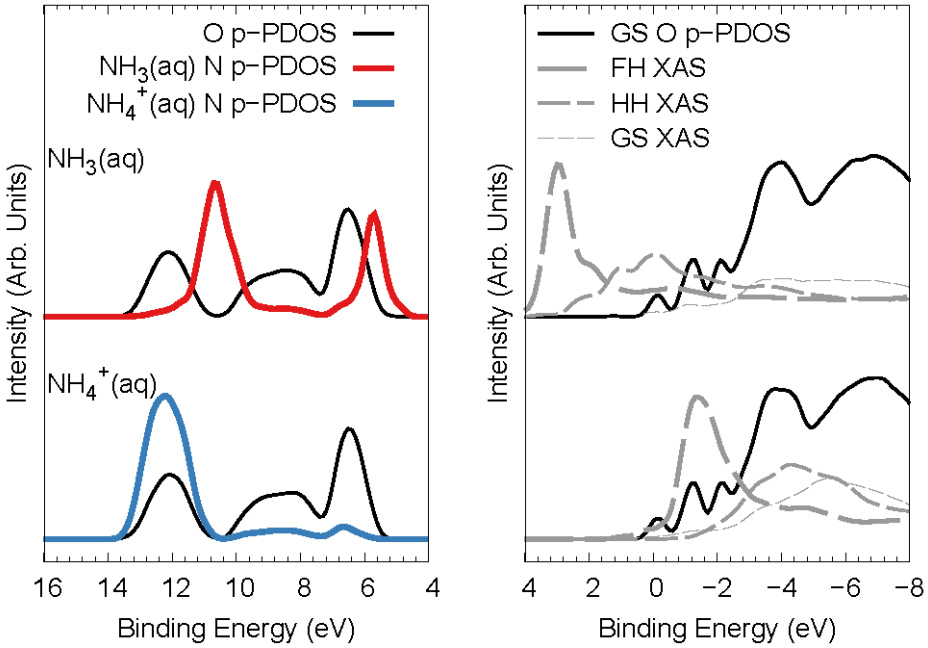

Table Of Contents Graphic

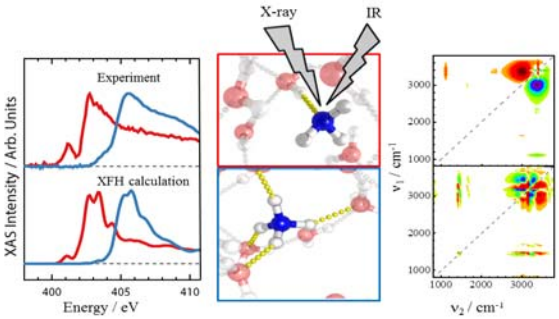

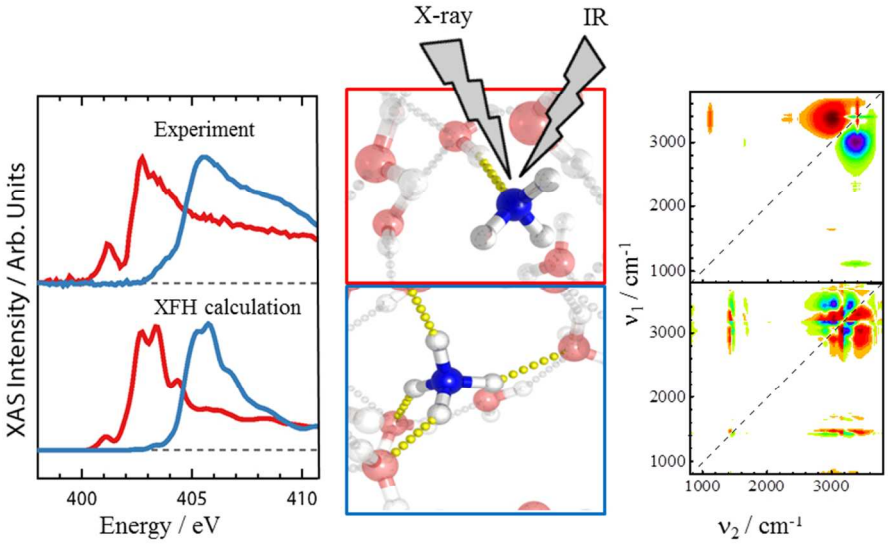

TOC-Graphic (TIFF file)

252x148mm (96 x 96 DPI)

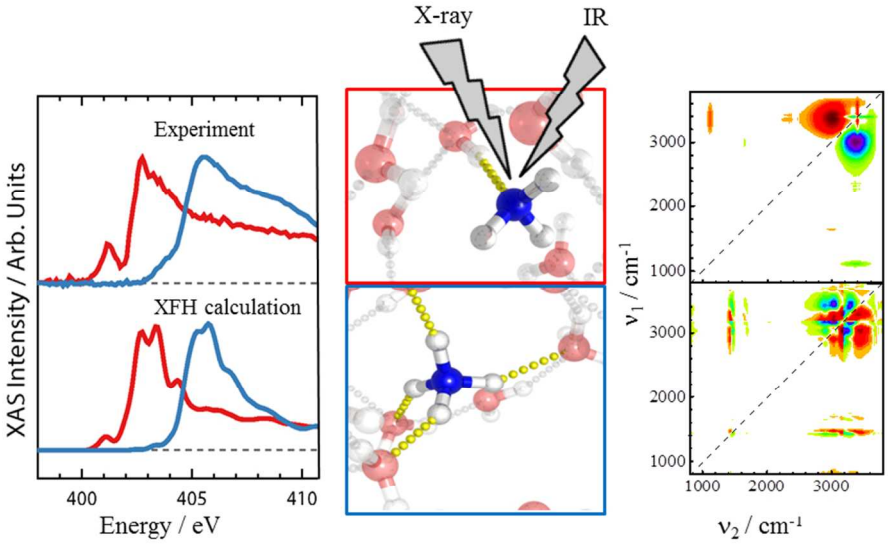

80x47mm (300 x 300 DPI)